Eur. Phys. J. C 9, 601–609 (1999)
Digital Object Identifier (DOI) 10.1007/s100529900096

THE EUROPEAN PHYSICAL JOURNAL C

Soft and hard Pomeron in the structure function of the proton at low x and low Q^2

U. D'Alesio, A. Metz, H.J. Pirner

Institut für Theoretische Physik, Universität Heidelberg, Philosophenweg 19, D-69120 Heidelberg, Germany

Received: 6 December 1998 / Revised version: 19 April 1999 / Published online: 18 June 1999

Abstract. We study inclusive electroproduction on the proton at low x and low Q^2 using a soft and a hard Pomeron. The contribution of the soft Pomeron is based on the Stochastic Vacuum Model, in which a nonperturbative dipole-dipole cross section can be calculated by means of a gauge invariant gluon field strength correlator. To model the hard Pomeron exchange we phenomenologically extend the leading order evolution of a power-behaved structure function, $F_2 \propto x^{-\lambda}$, proposed by López and Ynduráin. This extension allows to consider both the case $Q^2 = 0$ and the region of higher Q^2 on the basis of the same parametrization. A good simultaneous fit to the data on F_2 and on the cross section $\sigma_{\gamma p}$ of real photoproduction is obtained for $\lambda = 0.37$. With four parameters we achieve a $\chi^2/\text{d.o.f.} = 0.98$ for 222 data points. In addition, we use our model of the inclusive $\gamma^* p$ interaction to compute the longitudinal structure function F_L.

1 Introduction

Since the start of HERA exciting new information on the proton structure at very small x has been produced. Recently, the low x study has been extended to cover very small virtualities Q^2 [1,2]. This kinematical region is of particular interest because a transition from the purely perturbative scaling violations at large Q^2 to different physics at small Q^2 can be observed.

We consider the photon-proton collision in the *cm* frame. In this frame, the photon acquires a structure leading to the interaction of two structured objects. Accordingly, at least at high *cm* energy and low Q^2, the $\gamma^* p$ interaction has strong similarities to the hadron-hadron interaction. Our consideration of the soft Pomeron is based upon the fluctuation of the photon into a $q\bar{q}$ dipole. Higher Fock states (e.g. $q\bar{q}g$) in the wave function of the photon may lead to a hard Pomeron behaviour of the $\gamma^* p$ cross section.

In the framework of a model containing a soft and a hard Pomeron we perform in the present paper a fit to HERA data on F_2 together with data from NMC and E665 in a kinematical window given by $0.11\,\text{GeV}^2 \leq Q^2 \leq 6.5\,\text{GeV}^2$, $x \leq 0.01$, and $W \geq 10\,\text{GeV}$, with W representing the $\gamma^* p$ *cm* energy. Moreover, all data on the total absorption cross section $\sigma_{\gamma p}$ of real photons with $W \geq 10\,\text{GeV}$ are considered. The fit includes four free parameters. Our investigation is a natural extension of previous work [3], where F_2 at fixed W (20 GeV) has been studied as a function of Q^2. In [3] only a soft Pomeron contribution, derived in the Stochastic Vacuum Model (SVM) [4, 5], has been taken into account. The aim of the present paper is to study the importance of the soft Pomeron as given by the SVM in the low x and low Q^2 region of HERA.

The SVM is a specific model of nonperturbative QCD. It lives on the assumption that the infrared behaviour of QCD can be approximated by a Gaussian stochastic process. As central quantity of the SVM serves the correlator of the gluon field strength (nonlocal gluon condensate), which consists of an Abelian and a non-Abelian part, where the non-Abelian correlator gives rise to linear confinement in terms of the Wilson area law. Three parameters determine the correlator: the overall normalization is given by the local gluon condensate $\langle g^2 FF \rangle$, while the correlation length a fixes the shape of the correlator in coordinate space. Finally, the parameter κ regulates the relative weigth of the Abelian and the non-Abelian term. These parameters are proper quantities of nonperturbative QCD and can be obtained from lattice simulations. More details on the technical aspects of the SVM may be found e.g. in [6].

By means of the eikonal approximation an expression for the dipole-dipole scattering amplitude of the SVM has been derived [7]. Any diffractive reaction involving hadrons or photons can be calculated by means of the dipole-dipole amplitude and the wave functions of the particles. Besides studies on F_2 [3,8], the SVM has been applied to the hadron-hadron scattering [7,9,10], photo- and electroproduction of vector mesons [11,12] and of π^0 [13], and in a very recent work to the $\gamma^*\gamma^*$-interaction [14].

In the color-dipole picture of high-energy scattering the cross section depends on the sizes of the scattered particles. As a consequence, for instance the value of about

Correspondence to: A. Metz
(e-mail: metz@frodo.tphys.uni-heidelberg.de)

2/3 for the ratio of πp to pp total cross sections can naturally be explained by the different radii of π and p. Though the SVM gives a prediction for the dipole-dipole cross section as function of the dipole sizes, the resulting cross sections are energy-independent. In particular, the $s^{0.08}$ dependence of soft high-energy hadron-hadron scattering [15] does not follow from the SVM. (According to a recent work [16] a behaviour like $s^{0.094}$ gives a better fit to hadron-hadron cross sections.) Any energy-dependence of the scattering amplitude of the SVM has to be incorporated in a phenomenological way.

In order to explain the increase of F_2 at low x and finite Q^2 the soft Pomeron behaviour of hadron-hadron scattering is not sufficient. Therefore, in our treatment we keep the energy-independent prediction of the SVM as soft Pomeron and add, similar to other approaches (see e.g. [17,8]), a hard Pomeron component. For quite some time the BFKL-mechanism (exchange of a gluon-ladder) [18] has been considered as microscopic explanation of a hard Pomeron exchange. However, due to the poor convergence of this perturbative approach [19], the status of the BFKL-Pomeron is more than ever unclear. Because of this situation, and the fact that we are mainly interested in the behaviour of the soft Pomeron, we start from a simple ansatz for the hard Pomeron as derived by López and Ynduráin [20] and obtained by the leading order DGLAP evolution [21] of F_2. We modify the solution of the DGLAP equation by multiplying a phenomenological factor, leading to a parametrization which can be applied in the limit $Q^2 \to 0$ without introducing a singularity in the cross section of photoproduction. As a consequence of this modification our hard Pomeron component is no longer, strictly speaking, a solution of the DGLAP equation in the nonperturbative region of low Q^2.

In the analysis we neglect a contribution from meson exchange, being aware of the fact that at $W = 10\,\mathrm{GeV}$ the trajectories of a_2 and f_2 give rise to an effect of about 10%. Nevertheless, a consideration of the meson exchange introduces new parameters but has only minor influence on the main results of our investigation. Even though we make a fit to experimental data, we emphasize that in the present work we are not aiming at a fine-tuning of parameters.

2 Soft Pomeron

The structure function F_2 is given by the sum of the longitudinal and transverse total $\gamma^* p$ cross section in the form

$$F_2 = \frac{Q^2}{4\pi^2 \alpha_{QED}} (\sigma_L + \sigma_T)\,. \tag{1}$$

The relevant cross sections due to the soft Pomeron exchange have been calculated in [3] from the imaginary part of the forward amplitude for elastic $\gamma^* p$ scattering in the SVM. We obtain the result by summing over the flavours f of the $q\bar{q}$-fluctuation of the virtual photon,

$$\sigma_{L/T}^{SVM} = \sum_f \sigma_{f,L/T}^{SVM} = \sum_f e_f^2 \int_0^1 dz \int_{r_{cut}}^{\infty} dr\, r\, \mathcal{I}_{f,L/T}(z,r)\,, \tag{2}$$

where $e_f = \hat{e}_f e$ (e: elementary charge) denotes the charge of the different quark flavours. We take into account the three light quarks u, d, s. In (2) z is the longitudinal momentum fraction of the quark and r the modul of the two-dimensional vector $\mathbf{r} = r(\cos\vartheta, \sin\vartheta)$ between quark and antiquark. The use of a lower bound r_{cut} in the r-integration differs from the treatment in [3] and will be discussed in more detail below. The functions $\mathcal{I}_{f,L/T}(z,r)$ read

$$\begin{aligned}
\mathcal{I}_{f,L}(z,r) &= \frac{N_c}{4\pi^2}\, 4z^2(1-z)^2\, Q^2 K_0^2(\varepsilon_f r)\, J_p(z,r)\,, \\
\mathcal{I}_{f,T}(z,r) &= \frac{N_c}{4\pi^2}\Big\{[z^2 + (1-z)^2]\varepsilon_f^2 K_1^2(\varepsilon_f r) \\
&\qquad + m_f^2\, K_0^2(\varepsilon_f r)\Big\} J_p(z,r)\,, \quad \text{with} \\
\varepsilon_f^2 &= z(1-z)\, Q^2 + m_f^2 (Q_{eff}^2)\,.
\end{aligned} \tag{3}$$

These quantities are obtained from the absolute square of the virtual photon light cone wave functions, which contain the modified Bessel functions K_0 and K_1. $J_p(z,r)$ represents the soft Pomeron induced cross section for scattering of a $q\bar{q}$ color dipole of size r off the proton target in the SVM [11]. For a general dipole-proton cross section the expressions in (3) are identical to those given in [22]. In our approach $J_p(z,r)$ can be written as

$$\begin{aligned}
J_p(z,r) = 2 \int_0^{2\pi} d\vartheta \int_0^{\infty} db\, b \int_0^1 dz_p \int \frac{d^2\mathbf{r}_p}{4\pi} \\
\times |\psi_p(r_p)|^2\, J(b,z,\mathbf{r},z_p,\mathbf{r}_p)\,,
\end{aligned} \tag{4}$$

with b denoting the impact parameter between the color dipoles of the photon and proton. For simplicity we consider the proton in the quark-diquark picture and make use of a Gaussian wave function,

$$\psi_p(r_p) = \frac{\sqrt{2}}{S_p} e^{-r_p^2/4S_p^2}\,. \tag{5}$$

The extension parameter S_p in (5) and the *rms* radius of the proton are related according to $S_p = 2r_{p,rms}/\sqrt{3}$.

The quantity $J(b,z,\mathbf{r},z_p,\mathbf{r}_p)$ in (4) is the interaction amplitude for the scattering of two color dipoles. In the SVM, J depends only very weakly on the momentum fractions z and z_p. For small dipole sizes r and r_p one can completely neglect this dependence in J, and hence also in J_p. For small r, the dipole-proton cross section shows the typical dipole-behaviour, $J_p(z,r) \propto r^2$, while for larger values of r the cross section is no longer proportional to r^2. Around 1 fm for instance, one obtains a shape like $r^{1.5}$ [11].

The SVM relates the dipole-dipole amplitude J in the nonperturbative gluonic vacuum to the nonlocal gluon condensate. For details about the computation of J we refer the reader to the literature (see e.g. [7,11]). Here

we only specify the field strength correlator. Assuming that $\langle F^a_{\mu\nu}(z;w)F^b_{\rho\sigma}(0;w)\rangle$ does not depend crucially on the choice of the common reference point w, the most general form of the correlator reads

$$g^2\langle F^a_{\mu\nu}(z;w)F^b_{\rho\sigma}(0;w)\rangle = \frac{\delta^{ab}}{N_C^2-1}\frac{1}{12}\langle g^2FF\rangle \times\Big\{\kappa(g_{\mu\rho}g_{\nu\sigma}-g_{\mu\sigma}g_{\nu\rho})D(z;a) +\frac{1}{2}(1-\kappa)\Big[\partial_\mu(z_\rho g_{\nu\sigma}-z_\sigma g_{\nu\rho}) +\partial_\nu(z_\sigma g_{\mu\rho}-z_\rho g_{\mu\sigma})\Big]D_1(z;a)\Big\}. \quad (6)$$

The first tensor structure of the correlator is of non-Abelian type and leads to confinement, whereas the second term is an Abelian tensor. The shape of the correlation functions $D(z;a)$ and $D_1(z;a)$ is governed by the correlation length a.

It is now obvious that the size of the dipole-proton cross section $J_p(z,r)$ is given by the parameters of the field strength correlator ($\langle g^2FF\rangle$, a, κ) and the extension parameter S_p of the proton. The quantity κ is taken from a lattice simulation [25], while the remaining three parameters are fixed by the experimental values of the total pp cross section and the slope of the differential pp cross section, both taken at a cm energy of 20 GeV, and in addition by the phenomenological $q\bar{q}$-string tension $\rho = 8\,\kappa\,a^2\langle g^2FF\rangle/81\pi$. To be explicit we adopt the values [11],

$$\langle g^2FF\rangle = 2.49\,\mathrm{GeV}^4\,,\ a = 0.346\,\mathrm{fm}\,,\quad \kappa = 0.74\,,\ S_p = 0.74\,\mathrm{fm}\,. \quad (7)$$

In (3) ε_f denotes the extension parameter of the photon. It depends on the quark flavour through the quark mass, and thus each flavour contributes in a different way to the integrands $\mathcal{I}_{f,L/T}$. A crucial quantity in $\mathcal{I}_{f,L/T}$ is the Q^2-dependent quark mass. For large values of Q^2, the hadronic component of the photon is a free $q\bar{q}$ pair, while at lower Q^2 usually vector meson dominance (VMD) is used. In our approach, the photon is represented by a $q\bar{q}$ fluctuation over the whole region of Q^2. This picture of the photon has been studied in detail in [3] and leads automatically to an effective quark mass interpolating between a constituent quark and a current quark. Making use of quark-hadron duality the effective quark mass can be derived by comparing the phenomenological photon polarization tensor, which is obtained from VMD-poles and the perturbative continuum, with the polarization tensor we get in our description of the photon. Since in the photon wave function Q^2 appears together with the factor $z(1-z)$, the quark mass has been investigated as function of $Q^2_{eff} = 4z(1-z)\,Q^2$. The parametrization of the light quarks is [3]

$$m_{u/d}(Q^2_{eff}) = R\cdot 0.22\,(1-Q^2_{eff}/Q^2_{0,u/d})\,\mathrm{GeV}\,, \quad \text{for } Q^2_{eff}\le Q^2_{0,u/d} = 0.69\,\mathrm{GeV}^2\,,$$
$$m_{u/d}(Q^2_{eff}) = 0\,,\ \text{for } Q^2_{eff}\ge Q^2_{0,u/d}\,, \quad (8)$$

while for the strange quark one gets

$$m_s(Q^2_{eff}) = R\cdot[0.15+0.16\,(1-Q^2_{eff}/Q^2_{0,s})]\,\mathrm{GeV}\,, \quad \text{for } Q^2_{eff}\le Q^2_{0,s} = 1.16\,\mathrm{GeV}^2\,,$$
$$m_s(Q^2_{eff}) = R\cdot 0.15\,\mathrm{GeV}\,,\ \text{for } Q^2_{eff}\ge Q^2_{0,s}\,, \quad (9)$$

with a parameter $R = 1$. In previous works on inclusive scattering [3] and on vector meson production [12] the cross sections induced by real photons have always been too low by about 10−15%. This drawback can be removed by lowering the quark masses. Therefore, in our numerical calculation we take $R = 0.87$ which gives us the best fit to the data. The mass reduction of 13% is probably within the error bars which the values of m_f in (8,9) actually have.

For the lower bound of the r-integration in (2) we choose $r_{cut} = a$. Our hard Pomeron already describes the physics of small color dipoles, even though we do not yet have a dipole-formula for the hard cross section. To keep at small distances the SVM part of the cross section in addition to the hard part certainly leads to a double counting in this region. Of course, our specific separation in soft and hard physics is to some extend arbitrary. In particular, one could try to improve the final result by fitting the value of r_{cut}, which introduces however a new parameter. Moreover, e.g. lattice data for the field strength correlator show a clear deviation from the specific correlator used in the SVM at distances below the correlation length (c.f. [26]), where the deviation is due to a manifest perturbative contribution. This means that in the correlator a transition between soft and hard contributions appears at distances of the order 0.3–0.4 fm. The cut of the SVM contribution is similar to the procedure proposed by Rueter [8] previously. Nevertheless, the low distance physics is described in a different way in both approaches.

3 Hard Pomeron

Also for the hard Pomeron in principle a dipole description with an improved photon wave function containing gluons in addition to the $q\bar{q}$ pair holds. The scattering of these gluons on the proton is by far not trivial, for their transverse momenta can be small. A procedure has to be developed to separate soft and hard contributions. As working hypothesis the gluons with small light cone energies (i.e. finite light cone momenta and small transverse momenta) are already in the parametrization of the gluon field strength correlator of the SVM. There remain only gluons with large light cone energies (i.e. very small light cone momenta and large transverse momenta). These may be treated perturbatively.

To model the contribution of the hard Pomeron we consider the evolution of a power-behaved F_2 as derived by López and Ynduráin [20]. Perturbative QCD implies that to leading order in the running coupling the singlet structure function is of the form

$$F_2^{\mathrm{pert}}(x,Q^2) = B_2\,\alpha_s(Q^2)^{-d_+(1+\lambda)}\,x^{-\lambda}\,,\ \text{where} \quad (10)$$

$$d_+(1+\lambda) = \frac{1}{\beta_0}\left(\frac{12}{\lambda} - 11 - \frac{2}{9}\right), \text{ and}$$
$$\beta_0 = 11 - \frac{2}{3}N_f\,,\ N_f = 3\,.$$

In (10) d_+ denotes the leading eigenvalue of the anomalous dimension matrix of the quark-singlet and gluon evolution kernel. The formula for d_+ is valid for λ close to zero. The quantities B_2 and λ are free parameters. Equation (10) can be applied only for small values of x and is based on a singular gluon input. We emphasize that (10) is compatible with Regge theory, since the intercept $(1+\lambda)$ of the hard Pomeron does not depend on Q^2.

While in [20] the expression (10) was used above $Q^2 = 3\,\mathrm{GeV}^2$, in a recent work Adel, Barreiro and Ynduráin [23] have proposed to analyse F_2 also for lower values of Q^2 on the basis of (10). However, in this case a phenomenological modification of (10) is required in order to get a finite cross section for photoproduction. One possible modification is given in [23]. The authors make use of a specific freezing of the strong coupling,

$$\alpha_s(Q^2) \to \frac{4\pi}{\beta_0 \ln\left((Q^2+\Lambda^2)/\Lambda^2\right)}\,. \tag{11}$$

Moreover, d_+ has to be replaced using the self-consistency equation

$$d_+(1+\lambda) = 1 + \lambda\,. \tag{12}$$

One can now show immediately that by means of (11,12) the total cross section of photoproduction

$$\sigma_{\gamma p} = \frac{4\pi^2\alpha_{QED}}{Q^2}\,F_2\bigg|_{Q^2=0} \tag{13}$$

is finite. In [23] (12) has been solved leading to $\lambda = 0.47$. In particular, in the case of photoproduction this value seems to be too large as will become obvious in the next section. Therefore, we also apply (12), but in contrast to [23] we keep λ as a free parameter in our fit.

In addition to this parametrization, we consider an alternative ansatz for the hard component F_2^{hard}. We multiply F_2^{pert} in (10) by the phenomenological factor $(Q^2/(Q^2+M^2))^{1+\lambda}$ and freeze the strong coupling in a way different from the expression in (11). According to that, the hard contribution reads

$$F_2^{\mathrm{hard}}(x,Q^2) = C_2\,\tilde{\alpha}_s(Q^2)^{-d_+(1+\lambda)}x^{-\lambda}\left(\frac{Q^2}{Q^2+M^2}\right)^{1+\lambda}, \tag{14}$$
$$\text{with } \tilde{\alpha}_s(Q^2) = \frac{4\pi}{\beta_0 \ln\left((Q^2+M^2)/\Lambda^2_{QCD}\right)}\,,$$

where we apply a conventional $\Lambda_{QCD} = 0.25\,\mathrm{GeV}$. To keep the number of free parameters as small as possible the same quantity M serves as freezing mass in $\tilde{\alpha}_s$ and as parameter in the factor $Q^2/(Q^2+M^2)$. Therefore, our ansatz for F_2^{hard} contains only three free parameters.
Formula (14) avoids a relation between the freezing mass and Λ_{QCD} in the strong coupling. At large Q^2, QCD evolution (to leading order) is restored, and no use of the approximation (12) has to be made. Because of these reasons we consider the parametrization (14) as the most natural phenomenological extension of (10) allowing us to interpolate between $Q^2 = 0$ and higher values of Q^2. Already in the past various authors (see e.g. [27,17]) have exploited terms of the type $Q^2/(Q^2+M^2)$ in order to reach the correct behaviour of F_2 at low Q^2.

4 Fitting inclusive photo- and electroproduction

The complete ansatz for the structure function reads

$$F_2 = F_2^{\mathrm{soft}} + F_2^{\mathrm{hard}}\,, \tag{15}$$

where the soft part F_2^{soft} represents the contribution of the SVM as discussed in Sect. 2. Experimental data for both $\sigma_{\gamma p}$ and F_2 are fitted through (15). In practice we fix F_2^{soft} from the SVM and fit the two sets of parameters $(B_2, \lambda, \Lambda$ or $C_2, \lambda, M)$ to the difference of the data and the soft Pomeron contribution. Since the evaluation of F_2^{soft} requires tedious multiple integrations, the only free parameter of the soft Pomeron (quantity R in (8,9)) is not actually fitted but rather optimized on a discrete set of numbers obtained in separate calculations.

For the data on F_2 we use the kinematical cuts $Q^2 \le 6.5\,\mathrm{GeV}^2$, $x \le 0.01$ and $W \ge 10\,\mathrm{GeV}$. The limitation in Q^2 is mainly due to the fact that the soft Pomeron part does not satisfy the DGLAP equation. Our expression for the hard Pomeron requires the cut in x. Since the scattering amplitude of the SVM is obtained from an eikonal approximation the limitation in W becomes mandatory. The fit contains 150 data points obtained at HERA [1,2,28,29], 8 data points from NMC [30] and 43 data points from E665 [31]. Furthermore, 21 photoproduction data [32,33] are included under the condition $W \ge 10\,\mathrm{GeV}$.

In the first parametrization a $\chi^2/\mathrm{d.o.f.} = 1.00$, i.e. a good description of the experimental data is achieved. In the calculation of χ^2 the systematic and statistical errors have been folded in quadrature. The resulting values of the parameters are

$$B_2 = 0.0268 \pm 6\%\,,$$
$$\lambda = 0.37 \pm 1\%\,,$$
$$\Lambda = 1.12\,\mathrm{GeV} \pm 2\%\,. \tag{16}$$

For the second parametrization the fit improves slightly. We obtain $\chi^2/\mathrm{d.o.f.} = 0.98$ with the parameters

$$C_2 = 0.0025 \pm 3\%\,,$$
$$\lambda = 0.37 \pm 1\%\,,$$
$$M = 1.02\,\mathrm{GeV} \pm 4\%\,. \tag{17}$$

Obviously, the quality of the two fits is very similar. The difference of both fit-functions becomes certainly more important as soon as data at higher values of Q^2 are

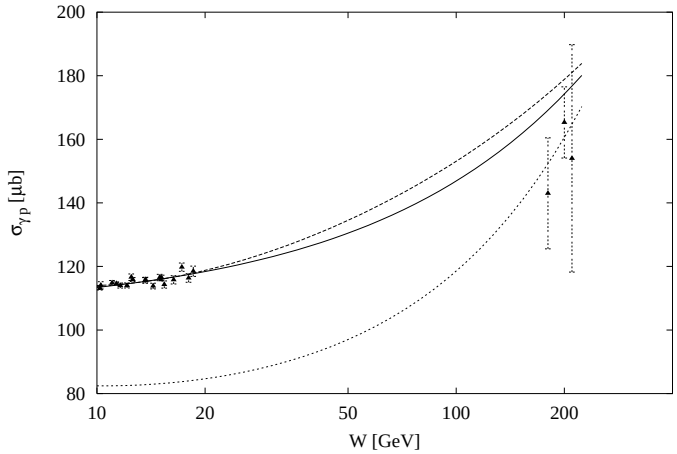

Fig. 1. Total cross section for real photoproduction. Low-energy experimental points are from [32], high-energy points are from [33]. Our fit (full line) is compared to those performed by Donnachie-Landshoff (dashed line) [17] and Adel-Barreiro-Ynduráin (dotted line) [23]

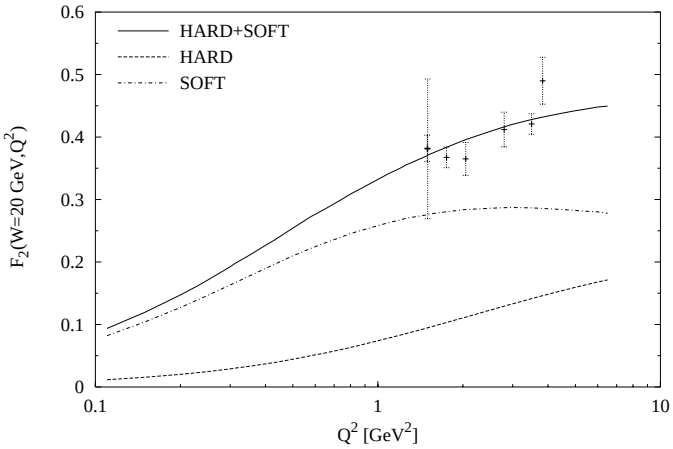

Fig. 2. Structure function F_2 at fixed $W = 20\,\text{GeV}$. The contributions of the soft and the hard Pomeron exchange are shown separately

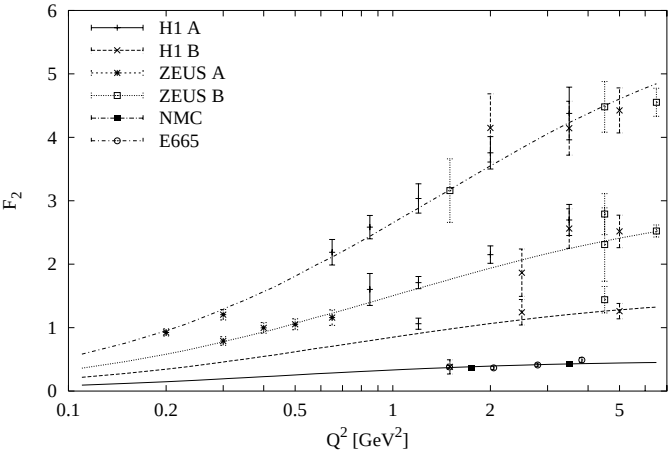

Fig. 3. F_2 vs Q^2 at fixed cm energy W, from bottom to top: $W = 20$ (×1), 60 (×2), 100 (×3), 200 (×4) GeV. The data points and curves are rescaled by the numbers in brackets. Experimental points are: H1 A [1], H1 B [28], ZEUS A [2], ZEUS B [29], NMC [30] and E665 [31]. The cm energies for the experimental points lie within a range of ±5% around the quoted numbers

involved. The errors of the parameters in (16,17) are very small. Our result for λ is on the lower edge of the recent result ($\lambda = 0.42$) obtained by Donnachie and Landshoff [17] and far below the value $\lambda = 0.47$ of [23]. The numbers of the saturation scales $\Lambda = 1.12\,\text{GeV}$ and $M = 1.02\,\text{GeV}$ are quite similar to the typical scale ($1.2 - 1.5\,\text{GeV}$) used in [27], and may be related to the lowest hadronic state having a $q\bar{q}g$ or $q\bar{q}q\bar{q}$ structure. These states could be considered as the entrance channel for the hard Pomeron.

In all numerical results we discuss in the following, our second ansatz including the parameters of (17) enters. We first consider the cross section for real photoproduction (see Fig. 1). The soft Pomeron gives rise to the energy-independent contribution $\sigma_{\gamma p}^{SVM} = 105.9\,\mu\text{b}$. This number depends crucially on the value of the constituent quark mass, where a reduction of the quark mass increases the cross section. In order to get in our two-component model a satisfying description of $\sigma_{\gamma p}$ for the whole energy range a reduction of the quark masses is unavoidable. The rise of $\sigma_{\gamma p}$ with increasing cm energy W is completely given by the hard Pomeron. This behaviour is different from the fit of Donnachie and Landshoff [17], where the hard Pomeron plays only a subordinate role in real photoproduction and the shape of $\sigma_{\gamma p}$ is mainly determined by the $s^{0.08}$ dependence of the soft Pomeron contribution.

The parametrization of Adel, Barreiro and Ynduráin [23] is similar to our approach. Contrary to us, these authors exploit for the soft Pomeron part in F_2 the simple VMD-inspired expression $Q^2/(Q^2 + \Lambda^2)$. Their fit, which includes data on F_2 down to $Q^2 = 0.32\,\text{GeV}^2$, can only describe the HERA data on $\sigma_{\gamma p}$ but underestimates the low energy data by about 35%. One reason of this shortcoming is certainly the high value $\lambda = 0.47$ adopted in [23].

We now consider the results for F_2 by focusing first on the Q^2-dependence of the structure functions at fixed W. Fig. 2, showing F_2 at $W = 20\,\text{GeV}$, demonstrates a good agreement with the experimental data. The hard and the soft contributions are shown separately. At low Q^2, both F_2^{soft} and F_2^{hard} are increasing with Q^2, where the soft part reaches a maximum around $2 - 3\,\text{GeV}^2$. Since at higher Q^2 the $q\bar{q}$ dipoles of the photon are dominantly small, the decrease of F_2^{soft} in this kinematical region is due to the lower bound r_{cut} in the integration over the dipole sizes. We emphasize that the shape of F_2^{soft} has a strong similarity with the purely empirical finding of Donnachie and Landshoff [17]. It is interesting to note that the soft and the hard Pomeron exchanges give sizable contributions for a relatively large range in Q^2. The hard Pomeron leads already at $Q^2 = 1\,\text{GeV}^2$ to an effect of about 25%, while on the other side the soft Pomeron part is at $Q^2 = 6\,\text{GeV}^2$ of the order 60% and therefore still very large.

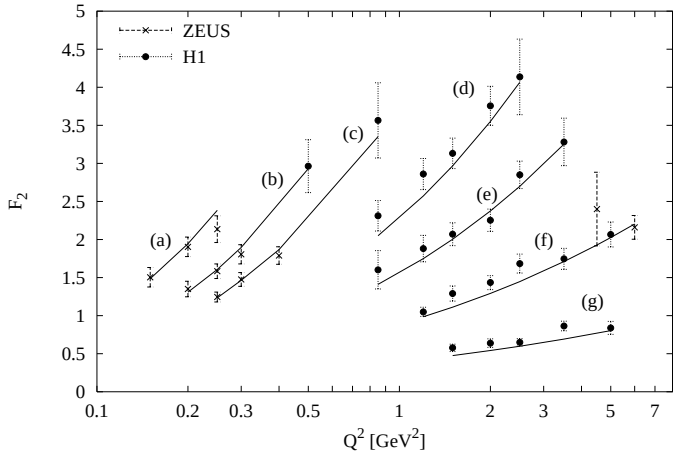

Fig. 4. F_2 vs Q^2 at different values of x. Experimental points at **a**, from left to right, $x = 0.42{\cdot}10^{-5}$, $x = 0.44{\cdot}10^{-5}$, $x = 0.46{\cdot}10^{-5}$ ($\times$ 8); **b**, from left to right, $x = 0.85{\cdot}10^{-5}$, $x = 0.84{\cdot}10^{-5}$, $x = 0.83 \cdot 10^{-5}$ and $x = 0.86 \cdot 10^{-5}$ ($\times$ 6); **c**, from left to right, $x = 0.13 \cdot 10^{-4}$ and three points at $x = 0.14 \cdot 10^{-4}$ ($\times$ 5); **d** $x = 0.5 \cdot 10^{-4}$ ($\times$ 4); **e** $x = 0.8 \cdot 10^{-4}$ ($\times$ 3); **f** $x = 0.2 \cdot 10^{-3}$ ($\times$ 2); **g** $x = 0.5 \cdot 10^{-3}$ ($\times$ 1). The data points and curves are rescaled by the numbers in brackets

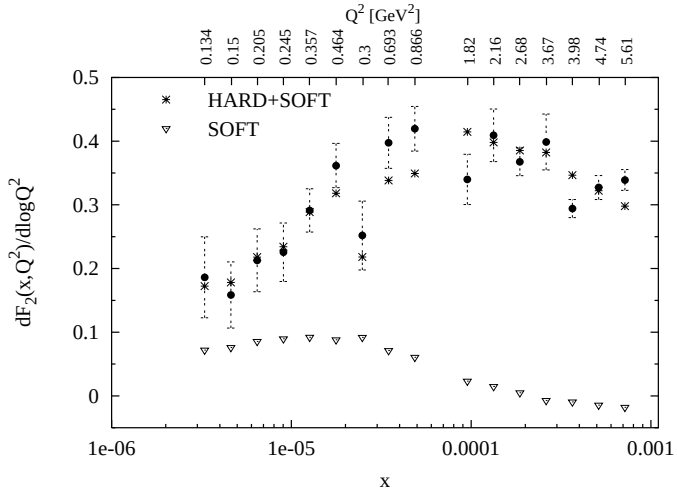

Fig. 5. Logarithmic derivative of F_2 vs x. Data points are from [34]. The soft contribution of the SVM is shown separately

To give an impression of the W-dependence, $F_2(Q^2)$ is shown in Fig. 3 for different cm energies. While $F_2^{\rm soft}$ is independent on W, the behaviour of the hard part is given by $F_2^{\rm hard} \propto 1/x^\lambda \approx (W^2/Q^2)^\lambda$. This leads to the fact that for high W the hard part dominates even at relatively low Q^2. In comparison with the case of $W = 20\,\mathrm{GeV}$ we find that for $W = 200\,\mathrm{GeV}$ the hard Pomeron contributes about 65% at $Q^2 = 1\,\mathrm{GeV}^2$ and 80% at $Q^2 = 6\,\mathrm{GeV}^2$.

In Fig. 4 we plot $F_2(Q^2)$ for various values of x concentrating on the region of HERA kinematics. This plot demonstrates that our model allows to fit the data for several orders of magnitude in x. To compare the relative contribution of the soft and the hard Pomeron exchange we consider here for convenience only the experimental point with the lowest value in x and Q^2 ($x = 0.42 \cdot 10^{-5}$, $Q^2 =$ 0.15). In this case the soft part turns out to be of the order 55%.

Finally, we discuss the logarithmic slope $dF_2/d\log Q^2$ as shown in Fig. 5, where the data points are taken from [34]. The experimental data in Fig. 5 are usually considered as proof of a breakdown of the perturbative scaling violations as given by the DGLAP equation [35] at a certain Q_0^2. However, as has been pointed out e.g. in [36], the value of Q_0^2 is strongly dependent on the specific selection of the experimental points. Our two-component model explains the data on the derivative quite well. The contribution of the SVM is shown separately in Fig. 5. At very low values of Q^2, the soft Pomeron gives rise to an effect of about 50%. This effect decreases with increasing Q^2 leading to a slightly negative value above $2 - 3\,\mathrm{GeV}^2$. The shape of the soft contribution just reflects the Q^2-dependence of the SVM part shown in Fig. 2.

5 Longitudinal structure function

Without introducing any new parameter we are now able to compute the longitudinal structure function F_L. Making use of the relation

$$F_L = \frac{Q^2}{4\pi^2 \alpha_{QED}}\,\sigma_L \tag{18}$$

and (2), the calculation of the SVM contribution is straightforward. The longitudinal cross section has to vanish in the limit $Q^2 \to 0$. In the SVM, where $\sigma_L \propto Q^2$ at low Q^2, this condition is automatically fulfilled.
To determine a hard component of F_L we proceed as follows. In perturbation theory the first nonvanishing contribution, arising from the QCD compton process and boson-gluon fusion, is given by [37],

$$F_L^{\rm pert}(x,Q^2) = \frac{\alpha_S(Q^2)}{2\pi} x^2 \int_x^1 \frac{dy}{y^3}\left[\frac{8}{3}F_2^{\rm pert}(y,Q^2) + 4\sum_f \hat{e}_f^2\, y g(y,Q^2)\Big(1-\frac{x}{y}\Big)\right]. \tag{19}$$

The gluon density g in (19) is related to the gluon structure function $F_G^{\rm pert}$ via

$$N_f F_G^{\rm pert}(x,Q^2) = \sum_f \hat{e}_f^2\, x g(x,Q^2)\,. \tag{20}$$

For low values of x, in [23] both $F_G^{\rm pert}$ and $F_2^{\rm pert}$ have been determined on the same basis to leading order in the running coupling. The two structure functions are related according to

$$F_G^{\rm pert}(x,Q^2) = \frac{d_+(1+\lambda) - D_{11}(1+\lambda)}{D_{12}(1+\lambda)} F_2^{\rm pert}(x,Q^2)\,, \text{with}$$
$$D_{11}(n) = \frac{16}{3\beta_0}\left[\frac{1}{2n(n+1)} + \frac{3}{4} - n\sum_k \frac{1}{k(k+n)}\right],$$
$$D_{12}(n) = \frac{2N_f}{\beta_0}\frac{n^2+n+2}{n(n+1)(n+2)}\,. \tag{21}$$

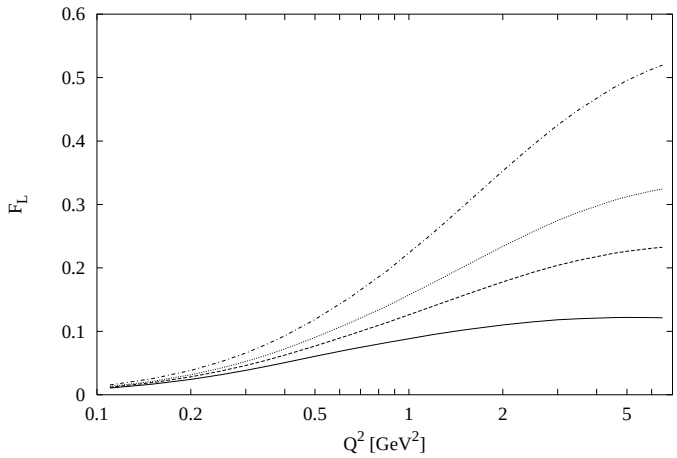

Fig. 6. F_L vs Q^2 at fixed cm energy W, from bottom to top: $W = 20$, 60, 100 , 200 GeV

The quantities D_{11} and D_{12} are matrix elements of the anomalous dimension matrix, and d_+ is the eigenvalue as defined in (10). By means of the expressions in (10,21) the structure function $F_L^{\rm pert}$ can easily be calculated. To get a hard component of F_L with an appropriate behaviour at low Q^2 we modify the perturbative result in the same spirit as we have done in (14) for F_2. This means, we multiply $F_L^{\rm pert}$ by the factor $(Q^2/(Q^2+M^2))^{2+\lambda}$, and moreover use the coupling $\tilde{\alpha}_s$ in (14). Therefore, we finally obtain

$$F_L^{\rm hard}(x,Q^2) = \frac{C_2}{2\pi(2+\lambda)}\tilde{\alpha}_s(Q^2)^{-d_+(1+\lambda)+1}x^{-\lambda} \qquad (22)$$
$$\times\left[\frac{8}{3}+\frac{4N_f}{3+\lambda}\frac{d_+(1+\lambda)-D_{11}(1+\lambda)}{D_{12}(1+\lambda)}\right]\left(\frac{Q^2}{Q^2+M^2}\right)^{2+\lambda}.$$

Obviously, by construction the behaviour of $F_L^{\rm hard}$ and $F_L^{\rm soft}$ at low Q^2 coincides since both are proportional to Q^4 near the real photon point.

In Fig. 6 we plot F_L as function of Q^2 for different values of the cm energy W. At higher values of Q^2, the decrease of the energy-independent soft contribution $F_L^{\rm soft}$ is more marked than in the case of F_2. This behaviour arises since the $q\bar{q}$ dipole of a longitudinal photon, in average, is smaller than the hadronic fluctuation of a transverse photon. As a consequence, at $W = 200\,\text{GeV}$ and $Q^2 = 6\,\text{GeV}^2$ the hard component exhausts almost 95% of the total result.

To compare our results with data we calculate the ratio $R_{LT} = \sigma_L/\sigma_T$, which is the observable usually measured in experiments. In terms of the soft and hard components of F_L and F_2 this ratio can be written as

$$R_{LT} = \frac{F_L^{\rm soft}+F_L^{\rm hard}}{(F_2^{\rm soft}-F_L^{\rm soft})+(F_2^{\rm hard}-F_L^{\rm hard})}. \qquad (23)$$

In the kinematical region of our fit there exist two data points from the NMC experiment [30]. As can be seen in Tab. 1, our results agree fairly with these data. The agreement obviously adds confidence to our approach, even if it is clear that we are not able to really test the model with only two data points.

Table 1. Comparison of the ratio R_{LT} in (23) with data points from [30]

x	$Q^2\,[\text{GeV}^2]$	R_{LT}^{exp}	R_{LT}
0.0045	1.38	0.537 ± 0.129	0.374
0.0080	1.31	0.337 ± 0.120	0.347

6 Summary and discussion

We have presented a two-component model for inclusive $\gamma^* p$ scattering, which consists of a soft and a hard Pomeron and is suitable in the region of low x and low Q^2. The four free parameters of the model have been adjusted to the available data on the structure function F_2 of the proton (for $0.11 \le Q^2 \le 6.5\,\text{GeV}^2$, $x \le 0.01$, $W \ge 10\,\text{GeV}$) and on the total cross section of real photoabsorption (for $W \ge 10\,\text{GeV}$). The fit includes 222 data points and leads to the result $\chi^2/\text{d.o.f.} = 0.98$.

The soft Pomeron has been calculated from the Stochastic Vacuum Model, which can be considered as an approximation of QCD in the infrared region. The SVM describes the complicated structure of the QCD vacuum in terms of a nonlocal gluon condensate, where the variation of the condensate in Minkowski space-time is governed by the correlation length a. In the framework of the SVM, diffractive scattering of two particles is equivalent to the scattering of two Wegner-Wilson-loops, leading automatically to cross sections in the color-dipole picture. To fix the distribution of the loops in the transverse space, valence quark wave functions of the particles have to be introduced.

The wave function of the photon has been determined in perturbation theory and accounts for the fluctuation of the γ^* into a $q\bar{q}$ state. This description differs from VMD frequently used in the region of low Q^2. A reasonable simultaneous description of F_2 and $\sigma_{\gamma p}$ for low and high W by means of VMD is difficult, and requires in general further parameters. VMD of the photon enters in our picture only through the determination of the quark masses by quark-hadron duality [3], and hence in a indirect way.

The soft Pomeron contains only one free parameter which regulates the overall normalization of the Q^2-dependent quark masses in the photon wave function. Compared to previous work on F_2 at fixed $W = 20\,\text{GeV}$ [3], performed only with a soft Pomeron, our fit favors a reduction of the quark masses by 13%. Such a reduction improves also e.g. the cross section for photoproduction of ρ-mesons [12]. The remaining (four) parameters of the soft Pomeron have been taken from other sources and left unchanged [11].

The cross sections of the SVM are energy-independent, contrary to the $s^{0.08}$ behaviour of the soft Pomeron in hadron-hadron scattering. To describe the data on F_2 obtained in fixed-target experiments and at HERA a hard Pomeron has to be considered in addition. We have modeled a hard component by starting from the leading order QCD evolution of a power-behaved structure function F_2 ($F_2 \propto x^{-\lambda}$) [20]. Assuming a singular gluon input, the

evolution does not produce a Q^2-dependence in the intercept, and hence the result is not in conflict with Regge theory. The result of the evolution has been multiplied by a simple phenomenological factor in order to obtain a finite cross section for real photoproduction. Our fit leads to $\lambda = 0.37$, which is close to a recently proposed value ($\lambda = 0.42$) by Donnachie and Landshoff [17].

The parameters of the fit have been used to calculate also the longitudinal structure function. Like in the case of F_2 we have to modify the perturbative part of F_L, which serves as starting-point for the hard component, by a phenomenologal factor in order to enforce a vanishing σ_L at $Q^2 = 0$. The numbers for the ratio $R_{LT} = \sigma_L/\sigma_T$ are in good agreement with two data points from the NMC experiment. Up to now there exist no HERA data in the kinematical region of our fit. However, recent activities at HERA will provide very soon final results from a direct measurement of F_L at low Q^2 [38].

During the last time many people investigated F_2 at low x and especially at low Q^2 with different models. The approaches comprise shadowing effects, Pomerons with a Q^2-dependent intercept, VMD calculations in combination with perturbative evolution and others (see e.g. [39–47]). Moreover, two-component Pomeron models have been applied to the $\gamma^* p$ interaction by various authors [23,48,49,36,17,8]. With a soft and a hard Pomeron Donnachie and Landshoff [17] presented for a large kinematical region a very good fit to $\sigma_{\gamma p}$ and F_2 using 10 parameters. In this work not only the intercepts, but also the residues of both Pomerons were fitted. In contrast to this, the residue of our soft Pomeron has been fixed by the SVM and related to parameters of nonperturbative QCD. In addition, at higher values of Q^2, the residue of the hard Pomeron follows the (leading order) evolution of QCD.

Our work strongly overlaps with the approach of Adel, Barreiro and Ynduráin [23], since we are using essentially the same expression for the hard Pomeron. However, we differ in the way of performing the limit $Q^2 \to 0$ in the hard part and, in particular, in the ansatz of the soft Pomeron which is given by a single VMD-pole in [23]. The parametrization of [23], obtained by a fit to data on F_2, fails in describing the data on $\sigma_{\gamma p}$ at low cm energies.

The work of Rueter [8], where a good description of the $\gamma^* p$ interaction was achieved, is also based on the SVM and therefore closest to ours. As discussed in detail in Sect. 2, we cut the soft proton-dipole cross section below the correlation length $a = 0.346\,\mathrm{fm}$. The interaction of small dipoles is taken into account by the hard Pomeron. A transition between soft and hard physics at distances of the order of the correlation length is suggested by lattice calculations of the field strength correlator [26]. In [8] the treatment of the dipole-proton cross section also changes for $r < a$. Contrary to our approach, Rueter still makes use of the residue of the soft Pomeron in the region of $0.16 - 0.35\,\mathrm{fm}$, but multiplies for this kinematics the cross section by the energy-dependence of a hard Pomeron (intercept 1.28). Dipoles with an extension smaller than 0.16 fm are treated by perturbative two-gluon exchange.

The extension of our two-component model to large Q^2 still has to be analysed. Moreover, one has to study the consequences in the case that our soft contribution is multiplied by the energy-dependence of the soft Pomeron of hadron scattering. If the fit significantly improves we would interpret this result as a further hint that a soft Pomeron leading to a slight energy-increase is required not only in the interactions of hadrons but also in $\gamma^* p$ interaction.

Acknowledgements. We thank H.G. Dosch and M. Rueter for critical discussions. One of the authors (A.M.) thanks E. Berger and G. Kulzinger for useful discussions concerning the model of the stochastic vacuum. U. D'Alesio was funded through the European TMR Contract No. FMRX-CT96-0008: Hadronic Physics with High Energy Electromagnetic Probes. A. Metz has been supported by BMBF.

References

1. H1: C. Adloff et al., Nucl. Phys. B **497**, 3 (1997)
2. ZEUS: J. Breitweg et al., Phys. Lett. B **407**, 432 (1997)
3. H.G. Dosch, T. Gousset, H.J. Pirner, Phys. Rev. D **57**, 1666 (1998)
4. H.G. Dosch, Phys. Lett. B **190**, 177 (1987)
5. H.G. Dosch, Yu.A. Simonov, Phys. Lett. B **205**, 339 (1988)
6. H.G. Dosch, Prog. Part. Nucl. Phys. **33**, 121 (1994)
7. H.G. Dosch, E. Ferreira, A. Kraemer, Phys. Rev. D **50**, 1992 (1994)
8. M. Rueter, Eur. Phys. J. C **7**, 233 (1999)
9. M. Rueter, H.G. Dosch, Phys. Lett. B **380**, 177 (1996)
10. E.R. Berger, O. Nachtmann, Eur. Phys. J. C **7**, 459 (1999)
11. H.G. Dosch, T. Gousset, G. Kulzinger, H.J. Pirner, Phys. Rev. D **55**, 2602 (1997)
12. G. Kulzinger, H.G. Dosch, H.J. Pirner, Eur. Phys. J. C **7**, 73 (1999)
13. M. Rueter, H.G. Dosch, O. Nachtmann, Phys. Rev. D **59**, 014018 (1999)
14. A. Donnachie, H.G. Dosch, M. Rueter, Phys. Rev. D **59**, 074011 (1999)
15. A. Donnachie, P.V. Landshoff, Phys. Lett. B **296**, 227 (1992)
16. J.R. Cudell, K. Kang, S.K. Kim, hep-ph/9712235 (1997)
17. A. Donnachie, P.V. Landshoff, Phys. Lett B **437**, 408 (1998)
18. V.S. Fadin, E.A. Kuraev, L.N. Lipatov, Phys. Lett. B **60**, 50 (1975); Y.Y. Balitsky, L.N. Lipatov, Sov. J. Nucl. Phys. **28**, 822 (1978)
19. V.S. Fadin, L.N. Lipatov, Phys. Lett. B **429**, 127 (1998); M. Ciafaloni, G. Camici, Phys. Lett. B **430**, 349 (1998); D.A. Ross, Phys. Lett. B **431**, 161 (1998)
20. C. López, F.J. Ynduráin, Nucl. Phys. B **171**, 231 (1980)
21. Yu.L. Dokshitzer, Sov. Phys. JETP **73**, 1216 (1977); V.N. Gribov, L.N. Lipatov, Sov. J. Nucl. Phys. **15**, 78 (1972); G. Altarelli, G. Parisi, Nucl. Phys. B **126**, 298 (1977)
22. N.N. Nikolaev, B.G. Zakharov, Z. Phys. C **49**, 607 (1991)
23. K. Adel, F. Barreiro, F.J. Ynduráin, Nucl. Phys. B **495**, 221 (1997)

24. A. Donnachie, P.V. Landshoff, Z. Phys. C **61**, 139 (1994)
25. A. Di Giacomo, H. Panagopoulos, Phys. Lett. B **285**, 133 (1992)
26. E. Meggiolaro, Phys. Lett. B **451**, 414 (1999)
27. B. Badelek, J. Kwieciński, Phys. Lett. B **295**, 263 (1992)
28. H1: S. Aid et al., Nucl. Phys. B **470**, 3 (1996)
29. ZEUS: M. Derrick et al., Z. Phys. C **69**, 607 (1996); M. Derrick et al., Z. Phys. C **72** (1996) 399
30. NMC: M. Arneodo et al., Nucl. Phys. B **483**, 3 (1997)
31. E665: M.R. Adams et al., Phys. Rev. D **54**, 3006 (1996)
32. D.O. Caldwell et al., Phys. Rev. Lett. **40**, 1222 (1978)
33. H1: S. Aid et al., Z. Phys. C **69**, 27 (1995); ZEUS: M. Derrick et al., Phys. Lett. B **293**, 465 (1992); ZEUS: M. Derrick et al., Z. Phys. C **63**, 391 (1994)
34. A. Caldwell, DESY Theory Workshop, DESY (1997)
35. M. Glueck, E. Reya, A. Vogt, Z. Phys. C **67**, 433 (1995)
36. P. Desgrolard, A. Lengyel, E. Martinov, Eur. Phys. J. C **7**, 655 (1999)
37. G. Altarelli, G. Martinelli, Phys. Lett. B **76**, 89 (1978)
38. D. Eckstein, private communication (1999)
39. H. Abramowicz, A. Levy, hep-ph/9712415 (1997)
40. P. Desgrolard, L. Jenkovszky, F. Paccanoni, Eur. Phys. J. C **7**, 263 (1999)
41. A.D. Martin, M.G. Ryskin, A.M. Stasto, Eur. Phys. J. C **7**, 643 (1999)
42. D. Schildknecht, hep-ph/9806353 (1998)
43. A.B. Kaidalov, C. Merino, hep-ph/9806367 (1998)
44. A. Rostovtsev, M.G. Ryskin, R. Engel, Phys. Rev. D **59**, 014021 (1999)
45. K. Golec-Biernat, M. Wuesthoff, Phys. Rev. D **59**, 014017 (1999)
46. E. Gotsman, E. Levin, U. Maor, E. Naftali, Nucl. Phys. B **539**, 535 (1999)
47. W. Buchmueller, T. Gehrmann, A. Hebecker, Nucl. Phys. B **537**, 477 (1999)
48. N.N. Nikolaev, B.G. Zakharov, V.R. Zoller, JETP Lett. **66**, 138 (1997)
49. G. Kerley, G. Shaw, Phys. Rev. D **56**, 7291 (1997)